A.Gehrer, J.Woisetschläger, H.Jericha (1997) *Blade Film Cooling by Underexpanded Transonic Jet Layers*, Proc. ASME International Gas Turbine and Aeroengine Congress, Orlando, Florida, 97-GT-246

Blade Film Cooling by Underexpanded Transonic Jet Layers

Arno Gehrer Jakob Woisetschläger Herbert Jericha
Institute of Thermal Turbomachinery and Machine Dynamics
Graz University of Technology
Graz, Austria

ABSTRACT

The evolution of increasing turbine inlet temperature has led to the necessity of full-coverage film cooling for the first turbine vane and blade. A new approach using high speed wall jets for blade cooling has been proposed by the authors. In this paper a 2-D upwind-biased Navier-Stokes code is used to calculate the aerodynamic behaviour of these surface coolant jets in a linear cascade. Special emphasis is put on the investigation of the coolant flow around the leading edge. Various numerical results concerning the leading edge flow are presented in detail, showing a strong tendency of these jets to bend towards convex surfaces. Finally, Schlieren pictures taken at the Institute's transonic cascade on a 140mm chord length blade are presented for comparison.

NOMENCLATURE

Symbols:

$A^+=26$	constant for the turbulence model
l	mixing length
L	chord length
M	Mach number
P	total pressure coolant/total pressure main flow
P^*	critical pressure coolant/total pressure main flow
T	static temperature
T_0	total temperature
u,v,w	cartesian velocity components
x	chordwise coordinate
y	minimum distance to any wall
y^+	nondimensiomal distance from the wall
δ	boundary-layer thickness
κ	ratio of specific heats
ω	vorticity
μ_t	eddy viscosity
μ_0	laminar viscosity at stagnation

Indexes:

c	coolant
m	main flow
1	at inflow boundary

INTRODUCTION

The objective of this work is to investigate underexpanded jets for a novel turbine blade film cooling system in a linear cascade, especially their aerodynamic behaviour around the leading edge. Since these underexpanded jets have a strong tendency to bend towards the surface a higher cooling efficiency is expected due to the improved cooling film attachment.

The effect of air flows bending around curved surfaces is generally connected with the name "Coanda-effect" and originally describes subsonic flows attaching to the surface by their turbulent structure (e.g. Fernholz and Wille, 1971; Ameria and Dybbs, 1993).

Several experiments with underexpanded jets bending towards a convex surface have been performed and published (Gregory-Smith and Gilchrist, 1987; Gilchrist and Gregory-Smith, 1988; Gregory-Smith and Hawkins, 1991; Gregory-Smith and Senoir, 1994). These curved supersonic jets have a complex structure with compression and expansion waves in the underexpanded core of the jet, with an outer free shear layer of the jet and a boundary layer towards the surface.

Since these underexpanded jets bend towards convex surfaces it has been suggested (Jericha et al., 1995) that its use might be considered for high temperature turbine blade film cooling. Cooling slits are suggested instead of holes in order to preserve this major property and also to cover a large area of the blade.

A preliminary investigation was performed with an acrylic glass model of a cooling slit (Woisetschläger et. al. 1995) which then

provided the basis for a cooling slit design inside the linear blade cascade at the Institute of Thermal Turbomachinery and Machine Dynamics, TU Graz (s. fig. 1).

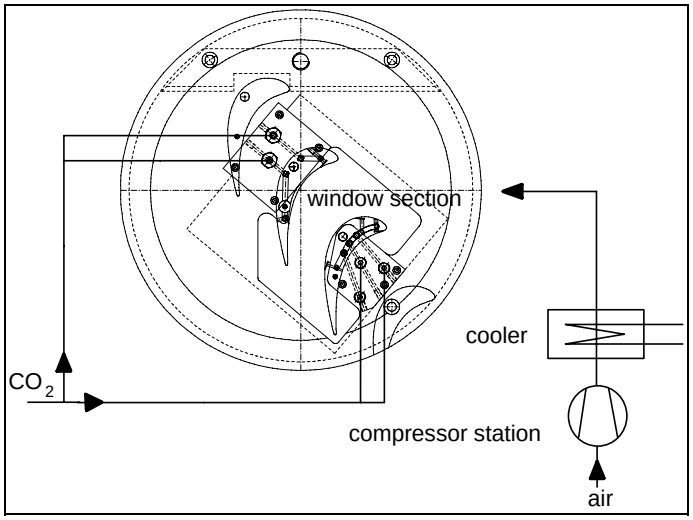

Fig. 1: Linear cascade, test section

The test section was designed to encompass a combined cycle proposed by Jericha et al. (1995) using high pressure steam as cooling medium for the high temperature gas turbine. In this case there would be no need of additional blowing energy. Since it is not possible to run the linear cascade test rig with the same flow temperatures as a real turbine an aerodynamically similar test section was designed using CO_2 as cooling flow medium. A detailed description of the measurement techniques has been given by Woisetschläger et al. (1996).

In the work presented here a 2-D Navier-Stokes code, based on the unsteady Euler code of Sanz et al. (1995), is used to demonstrate the effects described above and to investigate the influence of the supersonic cooling flow on the main flow field. For comparison with experimental data the blade profile and the slit geometry of the test section and the respective pressure ratios and temperatures have been investigated.

Since this Navier-Stokes code is limited to single-phase flow problems, the CO_2-flow in the cooling slit is calculated separately from the main flow. The respective results for velocity, pressure and density in the throat of the slit, where the average Mach number becomes unity, are then used as inflow boundary conditions for the main flow.

NUMERICAL METHOD

The unsteady, Reynolds averaged Navier Stokes equations are treated in conservative form and discretized in space using a cell-centred finite volume formulation with a quadrilateral structured cell system and in time using the Euler implicit method.

Inviscid Fluxes

On each cell boundary the inviscid fluxes are evaluated by an upwind scheme based on the approximate Riemann solver of Roe (1981). To raise the order of spatial accuracy the inviscid fluxes are evaluated using a 3rd order accurate TVD scheme. The TVD scheme is based on the MUSCL type of an upwind scheme which consists of a projection stage and an evolution stage. In the projection stage, left and right states at each cell interface are determined by extrapolating the cell-centred values of the conservative variables toward the cell interface according to the third-order upwind-biased scheme with a differentiable limiter (Anderson et al., 1985). In the evolution stage the inviscid flux is evaluated by solving the Riemann problem between left and right states using Roe's approximate Riemann solver. The implicit portions of the inviscid flux vectors are simplified by defining an approximation to the true linearization. Therefore, only a first order accurate scheme is considered for the implicit side whereas the full high-accuracy scheme on the explicit side is used (Sanz et al. 1995).

Viscous Fluxes

In order to construct the numerical viscous flux vector at the cell interfaces it is necessary to evaluate first-order derivatives of the velocity components and the sound speed, which is done in a central-differencing manner, using Green's theorem (e.g. Furukawa et al. 1991). The time linearization of the viscous flux vector is performed by applying the thin-layer approximation for the implicit side of the equations.

Turbulence Model

A two-layer algebraic model based on the mixing length concept is used for turbulence closure. In the near wall region the mixing length is computed using the Prandtl-Van Driest formula while in the outer region and in the wake it is kept constant to a fixed fraction of the shear layer thickness δ, according to the standard relation (Kwon et al, 1988).

$$l_{outer} = 0.085\,\delta$$

In the present work an algebraic criterion, which resembles the features of the Baldwin Lomax (1978) model, but which implicitly introduces a cut-off criterion for the vorticity field based on the distance from the wall, is used to estimate the boundary layer thickness (Arnone et al. 1996). If y denotes the distance normal to the wall, the value y_{max} at which the function

$$G(y) = \frac{1}{y}\int_0^y \bar{y}\omega\left(1 - e^{-\frac{\bar{y}^+}{A^+}}\right)d\bar{y}$$

reaches its maximum is assumed as turbulent length scale. The boundary layer thickness is then obtained from the relationship:

$$\delta = 1.145\, y_{max}$$

Boundary Conditions

In cascade-like configurations, there are four different types of boundaries: inlet, outlet, solid wall and periodicity. In the present cell-centred scheme, phantom cells are used to handle all boundaries. According to the theory of characteristics, flow angle, total pressure, total temperature and isentropic relations are used at the subsonic axial inlet, whereas all variables are prescribed at the supersonic inlet. At the subsonic axial outlet the average value of the static pressure is prescribed, density and velocity components are extrapolated, whereas all variables are extrapolated at supersonic axial outlet. On solid walls, the pressure is extrapolated from the interior points and the no-slip adiabatic condition is used to compute density and total energy.
The periodicity is imposed by setting periodic phantom cell values.

GEOMETRY, GRID SYSTEM

The blade profile with its cooling slits as it is built in the test section and the main design parameters are given in fig. 2. All calculations presented in this paper concentrate on the rather difficult situation near cooling slit #1, slits #2 and #3 are not subject of these investigations.

blade chord length	143 mm
blade pitch	98.6 mm
cooling slit throat	0.2 mm
design inlet angle*	55 °
design outlet angle*	28 °

* measured from circumferential direction

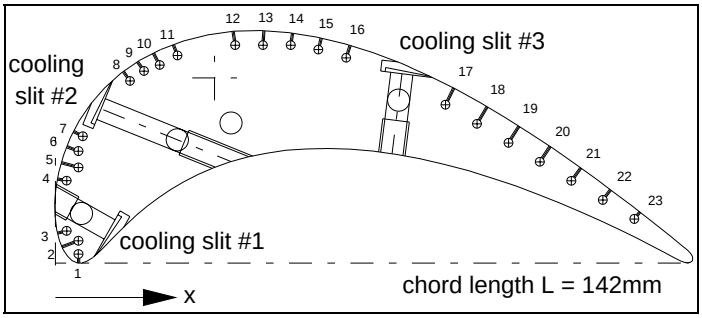

Fig. 2: Geometry of the blade and cooling slits

An algebraic mesh generator, developed by Gehrer et al. (1996), based on Bézier curves and Bézier surfaces was applied to generate a periodic C-type grid for the main flow field, which is shown in fig. 3. Two different grids were used to calculate the linear cascade flow.

Fig. 3.a shows the grid for the calculations without coolant which consists of 251 x 30 nodes. A refined version of this grid (s. figs. 3.b, 3.c), consisting of 274 x 40 nodes and including the throat of the cooling slit, is used to calculate the main flow with coolant.

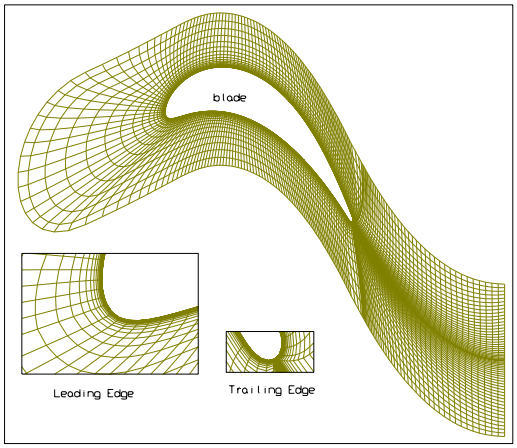

Fig. 3.a: Periodic C-type grid for the main flow without cooling jets (251 x 30 nodes)

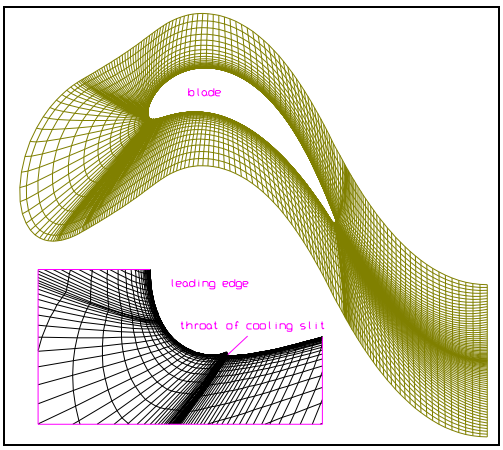

Fig. 3.b: Periodic C-type grid for the main flow with cooling jets (274 x 40 nodes)

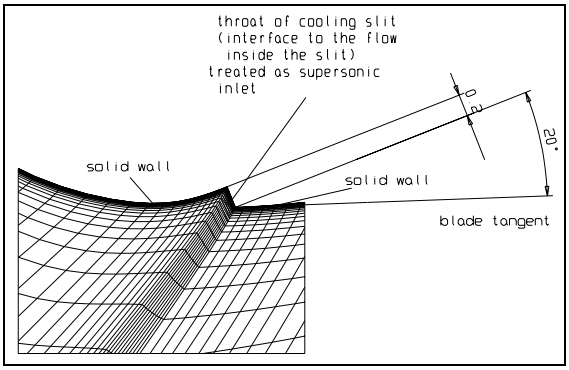

Fig. 3.c: Area around cooling slit

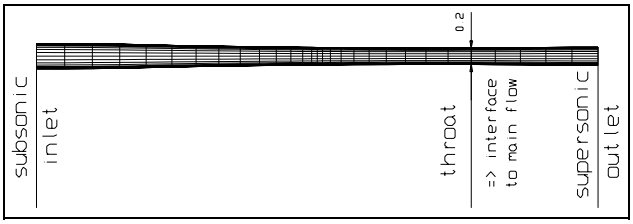

Fig. 3.d: Mesh for the flow inside the cooling slit (30x27 nodes)

Fig. 3.c shows the area around the cooling slit of the mesh in fig 3.b and finally fig. 3.d displays the mesh for the flow field inside the cooling slit (30 x 27 nodes).

RESULTS AND DISCUSSION

Three cases have been investigated. The respective boundary conditions, which were derived from experimental data, are given in table 1:

TABLE 1: Boundary conditions

			case1	case2	case3
			no coolant	P=2 P*=1.088	P=3 P*=1.632
main flow (air)	inlet	flow angle*	55°	55°	55°
		total pressure [bar]	1.211	1.211	1.211
		total temperature	40°C	40°C	40°C
	outlet	static pressure [bar]	1.015	1.015	1.015
coolant (CO2)	inlet	flow angle**	-	0°	0°
		total pressure	-	2.422	3.633
		total temperature	-	20°C	20°C
	outlet	supersonic outlet			

*measured from circumferential direction
**measured from the middle axis of the cooling slit

Numerical results, concerning mass flow, Reynolds numbers and exit flow angles are shown in table 2:

TABLE 2: Numerical Results

			case1	case2	case3
			no coolant	P=2	P=3
main flow	inlet	mass flow[kg/s/m]	9.47	9.34	9.17
	outlet	mass flow[kg/s/m]	9.47	9.46	9.36
		flow angle*	27.59°	27.39°	26.94°
		Reynolds number based on chord	1.65E+06	1.69E+06	1.71E+06
coolant		mass flow[kg/s/m]		0.12	0.19
		blowing ratio =(coolant mass flow /inlet mass flow)		1.32 %	2.04 %
		Reynolds number based on throat		9.37E+03	1.41E+04

*measured from circumferential direction

Results for the main flow without cooling jet (case1)

In order to validate the numerical results, in fig. 4.a, a comparison of calculation with experiment is presented. The isentropic blade surface Mach number distribution for the main flow without cooling jets shows reasonable agreement with experimental data. Furthermore, streamlines in the area of the leading edge (fig. 4.b), density contours (fig. 4.c) and pressure contours (fig. 4.d) illustrate the flow situation for case1.

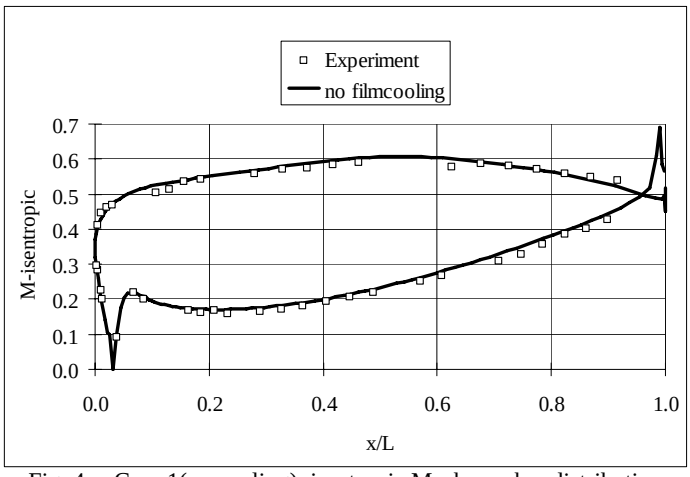

Fig. 4.a: Case 1(no cooling): isentropic Mach number distribution comparison with experiments

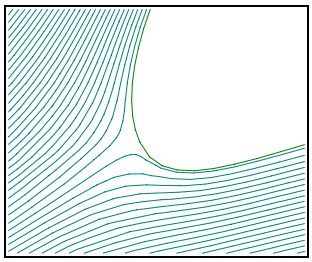

Fig. 4.b: Leading edge: streamlines for case 1

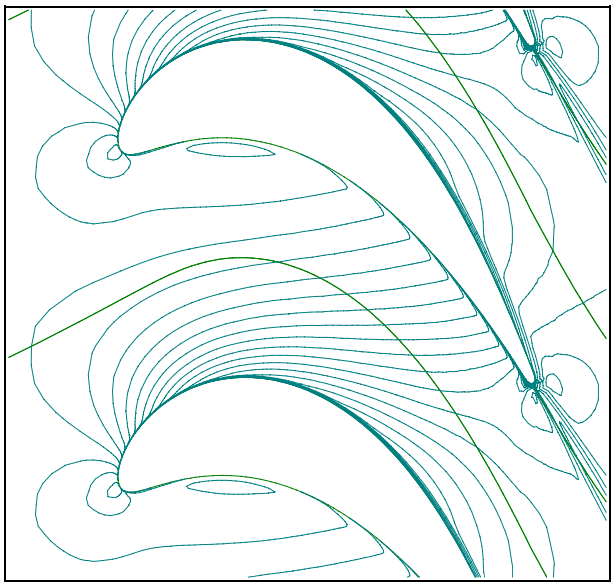

Fig. 4.c: Density contours for case 1

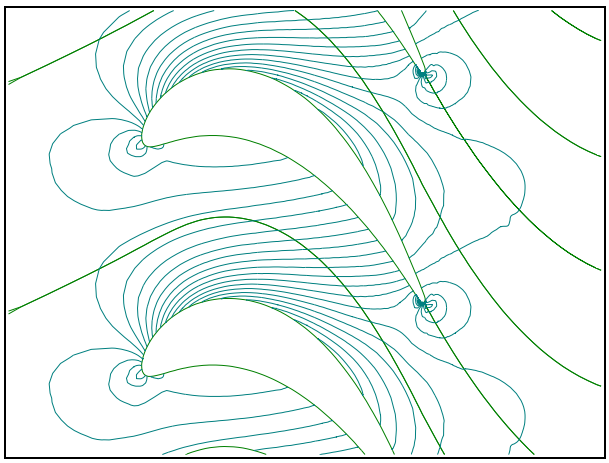

Fig. 4.d: Pressure contours for case 1

Results for the flow inside the cooling slit (e.g. case2)

In fig. 5 computational results for the CO_2 - flow inside the cooling slit (e.g. case 2) are presented.

Fig. 5.a: Cooling slit: Mach number contours

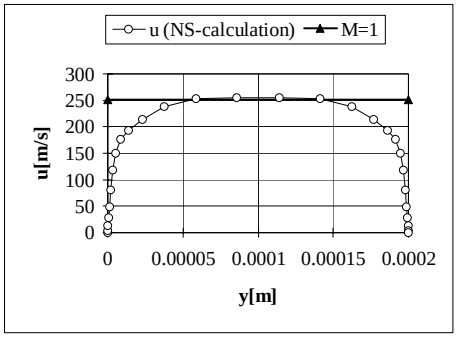

Fig. 5.b: Cooling slit: Velocity distribution across throat

In fig. 5.a the Mach number contours illustrate the growth of the boundary layer inside the slit, which is, due to the relatively low Reynolds number (s. table 2) of about 10^4, rather pronounced. In fig. 5.b, the velocity distribution across the throat of the slit is displayed. As mentioned above, the calculated velocity, density and pressure distributions across the throat (see also fig. 3.c) are prescribed as supersonic inflow boundary for the main flow for cases 2 and 3. However, the result for the supersonic part (throat to outlet in fig. 3.d) is not used for the main flow calculation. It should be noted that also the subsonic boundary layer region in the throat was treated as supersonic inflow boundary for the main flow.

Results for the main flow with cooling jet (cases 2 and 3)

Regarding the flow with coolant, the respective density contours in figs. 6.a and 6.b clearly demonstrate that it appears possible to keep the cooling layer close to the surface of the blade, even in the region of the highly curved leading edge radius and even in a direction opposite to the incoming flow.

The numerical results given in table 2 show a slight reduction of both inlet mass flow and exit flow angle, which indicates that the high speed cooling jet enhances the overall blade vortex.

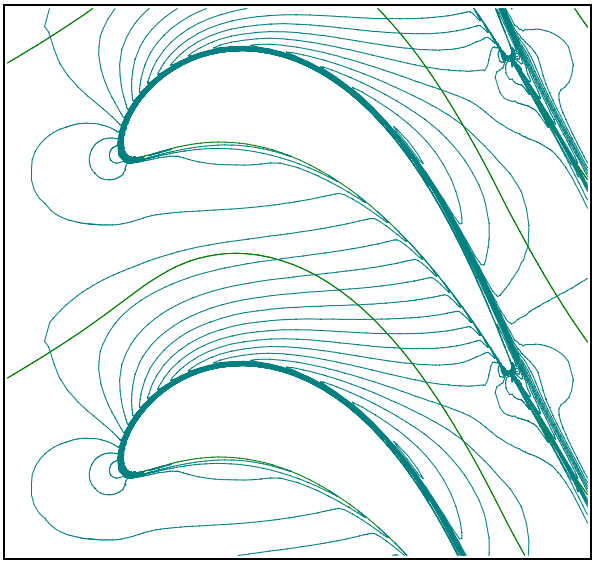

Fig. 6.a: Density contours for case 2

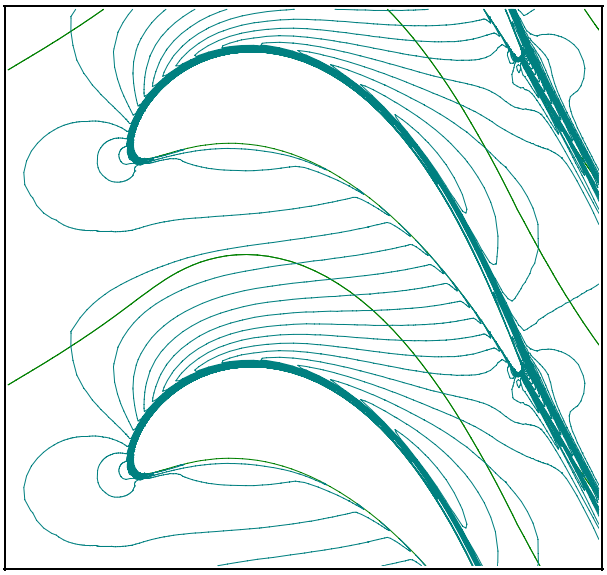

Fig. 6.b: Density contours for case 3

A more detailed view of the domain of interest in fig. 8 illustrates that the outflow of supersonic cooling medium from the slit forms a cooling layer around the leading edge of the blade. Especially the Mach number distributions in figs. 8.e and 8.f show that the jet expands to transonic velocities and, at the same time, due to the effect of continuous expansion, the film adheres very closely to the surface. This expansion can also be noticed as a pressure drop, which is clearly visible in the pressure contours.(s. figs. 8.a and 8.b).

For purpose of comparison, the Schlieren visualisation of the leading edge flow is presented in fig.7 which can be regarded as a qualitative verification of this effect.

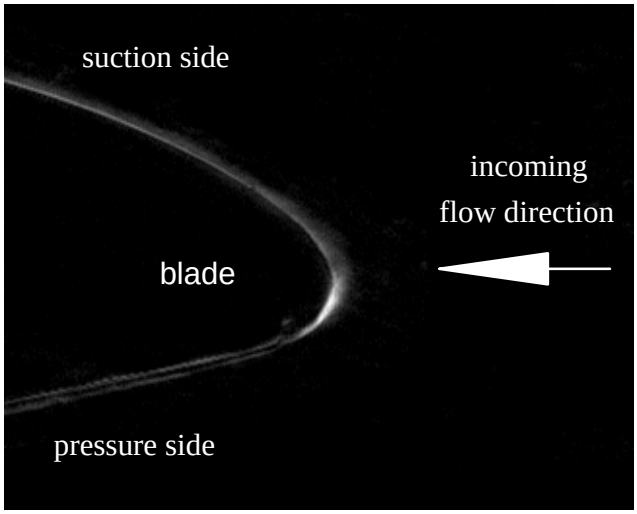

Fig. 7: Schlieren visualisation of the leading edge flow: main flow with the underexpanded cooling film at a pressure ratio of P = 2

Regarding the turbulent viscosity values in figs. 8.g, 8.h, it is obvious, that the outer free shear layer of the jet causes very high turbulence intensities which, especially in the region of opposite flow directions, are the main reason for rather high losses of kinetic energy in the underexpanded core of the jet. The streamlines in figs. 8.c and 8.d show a distinct vortex in this area.

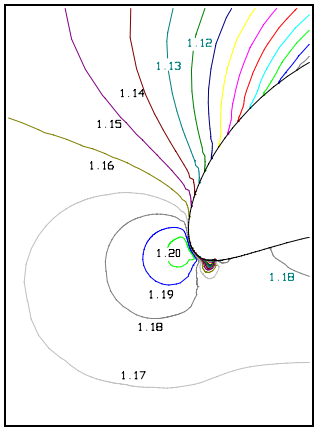

Fig. 8.a: Pressure contours, P=2 incremental step size: 0.01 bar

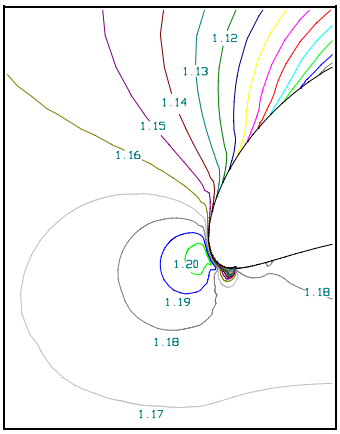

Fig. 8.b: Pressure contours, P=3

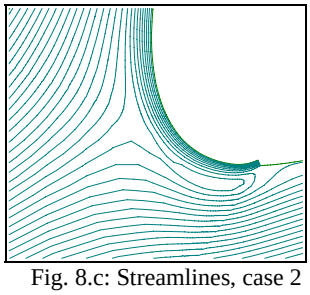

Fig. 8.c: Streamlines, case 2

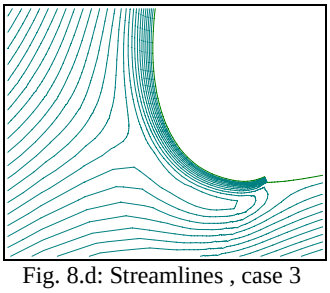

Fig. 8.d: Streamlines , case 3

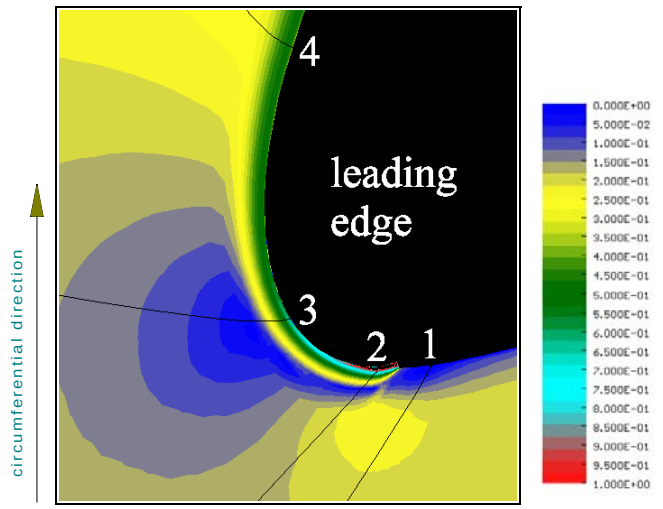

Fig. 8.e: Mach number distribution, case 2: M_{max} = 1.1446 (in the core of the jet). The gridlines, indicated by the numbers 1,2,3 and 4 have been used to evaluate the velocity profiles given in fig. 9.b.

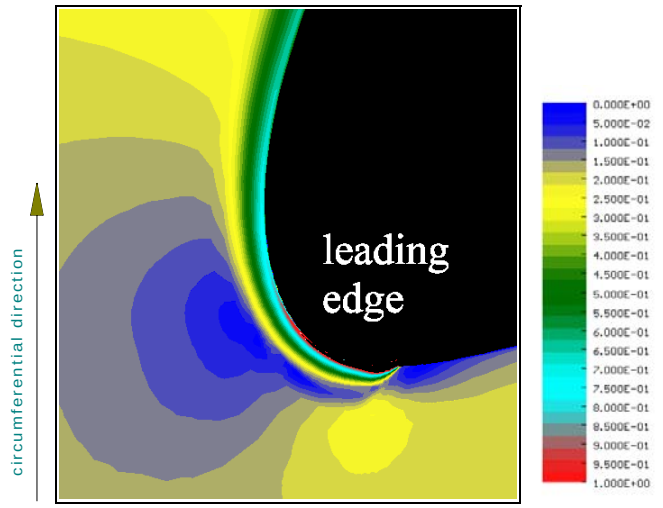

Fig. 8.f: Mach number distribution, case 3 M_{max} = 1.665 (in the core of the jet)

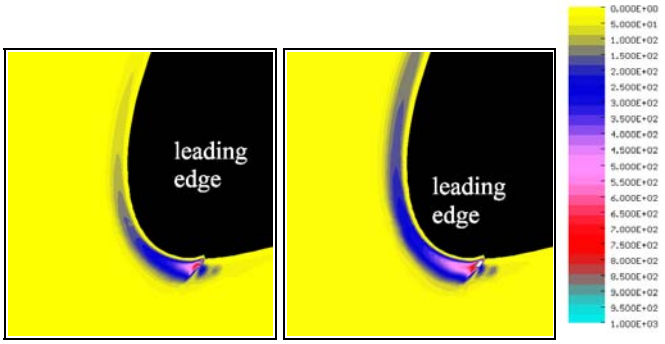

Fig. 8.g: Eddy viscosity (μ_t/μ_0) contours, P=2 $(\mu_t/\mu_0)_{max}$=1013

Fig. 8.h: Eddy viscosity (μ_t/μ_0) contours, P=3 $(\mu_t/\mu_0)_{max}$=1670

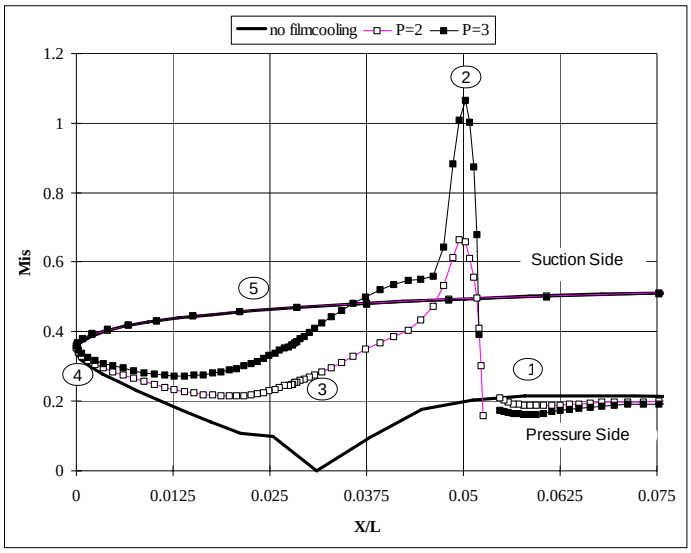

Fig. 9.a: Isentropic Mach number distribution in the area near the leading edge

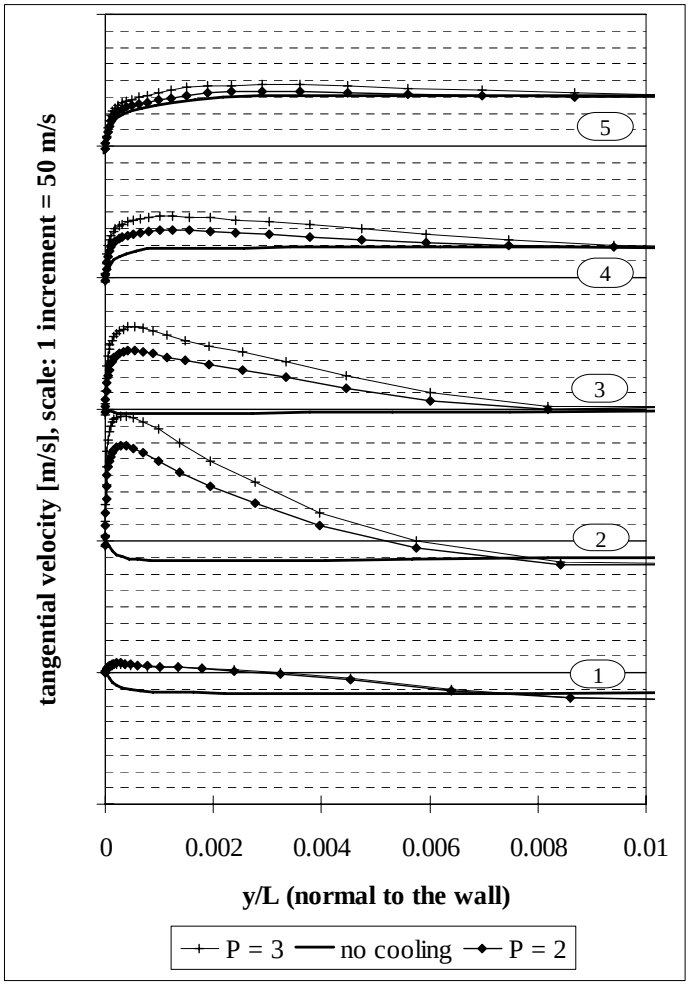

Fig. 9.b: Velocity profiles in the area of the leading edge. The respective locations are denoted by the numbers ①②③④⑤. These positions are also shown in figs. 8.e and 9.a.

The isentropic Mach number distribution in the area around the leading edge (s. fig. 9.a) shows a significant peak shortly after the coolant is injected at the pressure side of the blade. This means that the jets definitely accelerates the main flow (in flow direction of the jet) around the leading edge, which is also clearly visible in fig. 9.b, where the respective velocity profiles are given. The locations of gridlines used to evaluate these profiles are displayed in figs. 8.e and 9.a.

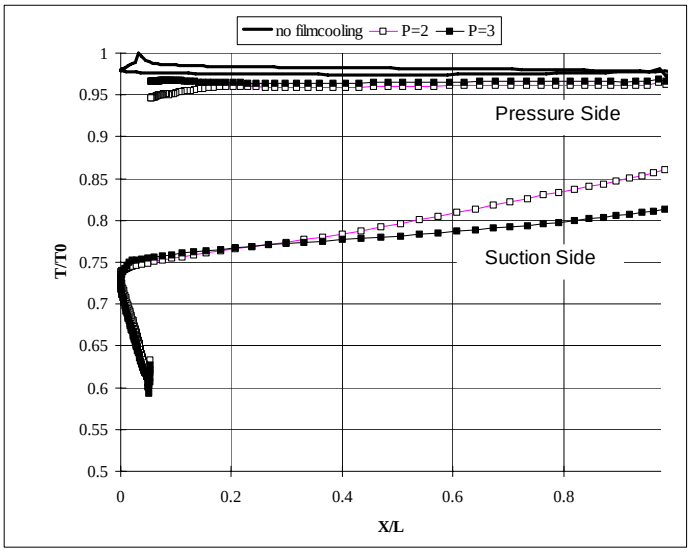

Fig. 10: Predicted temperature at the wall, normalised with the main flow total inlet temperature

Finally, the predicted temperature distribution at the (adiabatic) wall, normalised by the main flow total inlet temperature is presented (s. fig. 10). It should be kept in mind, that the results from the CO_2 flow calculations (total temperature, CO_2 : 293.15 K) inside the cooling slit were transferred to the main flow field (air), keeping the same pressure, velocity and density, which results in a total temperature of about 193 K. Under these conditions, the calculations predict, that the cold cooling jet fluid remains along the whole suction side, its temperature rises due to friction, heat transfer and mixing with the main flow.

Finally, it can be noticed, that all numerical results for case 3 are qualitatively similar to the results for case 2, which means that this range of pressure ratio P seems possible for a strong adherence between this type of cooling film and the blade surface. Investigations, presented by Gilchrist and Gregory-Smith (1988) and Woisetschläger et al. (1995), show that further increase of pressure ratio P leads to a low speed recirculation zone between jet and surface in the boundary layer which then causes a jet "breakaway" from the surface.

CONCLUSION

Underexpanded cooling films have a strong tendency to bend towards the surface which makes them interesting especially for cooling of the leading edge area. In this work, 2D Navier Stokes calculations were used to demonstrate, that transonic pressure ratios of P = 2 and 3 can provide a sufficient cooling layer around the leading edge area.

The respective computational results showed that these transonic wall jets adhere very closely to the surface, even in regions of opposite flow directions.

Ongoing numerical and experimental investigations will deal with velocity, turbulence and density changes due to underexpanded surface coolant films with and without upstream flow distortions. Furthermore these investigations are expected to provide data concerning the heat transfer and temperature situation.

These data then will be used to evaluate the whole cooled gas turbine or even the whole cycle thermodynamically in order to give a full answer concerning the amount of additional energy for blowing and aerodynamical losses compared to conventional film cooling.

ACKNOWLEDGEMENT

The authors gratefully acknowledge the support of the Austrian Science Foundation (FWF) supporting this research as well as ongoing research in efficiency improvement of thermal energy production.

REFERENCES

Ameria, M. and Dybbs, A., 1993, "Coanda ejector - why it works", *Proceedings of the SPIE, Vol 2052, pp 289-296*

Anderson, W. K., Thomas, J. L., Van Leer B. 1985 "A Comparison of finite Volume Flux Vector Splittings for the Euler Equations" *AIAA Paper No. 85-0122*

Arnone, A., Swanson, R.C. 1993 "A Navier Stokes Solver for Turbomachinery Applications" *Journal of Turbomachinery, April 1993, Vol. 115/305-313*

Arnone, A., Pacciani, R. 1996 "IGV-Rotor Interaction Analysis in a Transonic Compressor Using the Navier Stokes Equations", *ASME paper 96 - GT - 141*

Fernholz, A. and Wille, R., 1971, " Grenzschichten und Wandstrahlen an stark gekrümmten Wänden (COANDA-Effekt)", *DLR Forschungsbericht, FB71-46*

Furukawa, M., Yamasaki, M, Inoue, M, 1992 "A Zonal Approach for Navier Stokes Computations of Compressible Cascade Flow Fields Using a TVD Finite Volume Method", *Journal of Turbomachinery, Oct. 1992, Vol. 113/573-582*

Gehrer A., Paßrucker H., Jericha H., Lang J., 1996 "Blade design and Grid generation for Computational Fluid Dynamics (CFD) with Bézier-curves and Bézier-surfaces", *European Conference - Antwerpen - March '97, Paper No. 54*

Gilchrist, A.R. and Gregory-Smith, D.G. , 1988, "Compressible Coanda wall jet: predictions of jet structure and comparison with experiment", *International journal of Heat and Fluid Flow, Vol.9, pp 286-295*

Gregory-Smith D.G. and A.R.Gilchrist, 1987, "The compressible Coanda wall jet - an experimental study of jet structure and breakaway", *Heat and Fluid Flow, Vol. 8, pp 156-164*

Gregory-Smith D.G. and Hawkins,M., 1991, "The development of an axisymmetric curved turbulent wall jet", *International Journal of Heat and Fluid Flow, Vol.12, pp 323-330*

Gregory-Smith, D.G. and Senoir P., 1994, " The effects of base steps and axisymmetry on supersonic jets over coanda surfaces", *International Journal Heat and Fluid Flow, Vol.15, pp 291-298*

Jericha, H., Sanz, W., Woisetschläger, J and Fesharaki, M., 1995, "CO_2-Retention Capability of CH_4/O_2-Fired Graz Cycle", *Proceedings CIMAC 95, paper G07*

Kwon, O. K., Pletcher R. H., Delaney R. A. 1988 "Calculation of Unsteady Turbulent Boundary Layers" *Journal of Turboachinery, April 1988, Vol. 110, pp 195-201*

Roe P. L. 1981 "Approximate Riemann Solvers, Parameter Vectors and Differencing scheme", Journal of Computational Physics 43, 357 - 372

Sanz, W., Gehrer, A.,Paßrucker, H. 1995 "An Implicit TVD Upwind Relaxation Scheme for the Unsteady 2D-Euler-Equations" *ASME Paper 95 - CTP - 71*

Woisetschläger, J., Jericha, H., Sanz, W. and Gollner F., 1995, "Optical investigation of transonic wall-jet film cooling", *ASME Paper 95-CTP-26*

Woisetschläger J., Jericha H., Sanz W., Pirker H. P., Seyr A., Ruckenbauer T. 1996 "Experimental Investigations of Transonic Wall-Jet Film Cooling in a Linear Cascade", *European Conference - Antwerpen - March '97*